Are negative index materials achievable with surface plasmon waveguides? A case study of three plasmonic geometries

Jennifer A. Dionne,[1*] Ewold Verhagen,[2] Albert Polman,[2] and Harry A. Atwater[1]

[1]*Thomas J. Watson Laboratories of Applied Physics, California Institute of Technology, Mail Code 128-95, Pasadena, CA 91125, USA*

[2]*Center for Nanophotonics, FOM-Institute for Atomic and Molecular Physics (AMOLF), Kruislaan 407, 1098 SJ Amsterdam, The Netherlands*

[*]*Corresponding author: jdionne@caltech.edu*

Abstract: We present a theoretical analysis of planar plasmonic waveguides that support propagation of positive and negative index modes. Particular attention is given to the modes sustained by metal-insulator-metal (MIM), insulator-metal-insulator (IMI), and insulator-insulator-metal (IIM) geometries at visible and near-infrared frequencies. We find that all three plasmonic structures are characterized by negative indices over a finite range of visible frequencies, with figures of merit approaching 20. Moreover, using finite-difference time-domain simulations, we demonstrate that visible-wavelength light propagating from free space into these waveguides can exhibit negative refraction. Refractive index and figure-of-merit calculations are presented for Ag/GaP and Ag/Si_3N_4 - based structures with waveguide core dimensions ranging from 5 to 50 nm and excitation wavelengths ranging from 350 nm to 850 nm. Our results provide the design criteria for realization of broadband, visible-frequency negative index materials and transformation-based optical elements for two-dimensional guided waves. These geometries can serve as basic elements of three-dimensional negative-index metamaterials.

OCIS codes: (240.6680) Optics at surfaces; (160.3918) Materials: Metamaterials; (222.0220) Optical design and fabrication.

References and links

1. J. B. Pendry, D. Schurig, and D. R. Smith, "Controlling Electromagnetic Fields," Science **312**, 1780-1782 (2006).
2. D. Schurig, J. B. Pendry, and D. R. Smith, "Transformation designed optical elements," Opt. Express **15**, 14772-14782 (2007).
3. J. B. Pendry, "Negative Refraction Makes a Perfect Lens," Phys. Rev. Lett. **85**, 3966-3969 (2000).
4. N. Fang, H. Lee, C. Sun, X. Zhang, "Sub-diffraction-limited optical imaging with a silver superlens," Science **22**, 534-537 (2005).
5. T. Taubner, D. Korobkin, Y. Urzhumov, G. Shvets, and R. Hillenbrand, "Near-Field Microscopy Through a SiC Superlens," Science **313**, 1595 (2006).
6. Z. Jacob, L. A. Alekseyev, and E. Narimanov, "Optical Hyperlens: Far-field imaging beyond the diffraction limit," Opt. Express **14**, 8247-8256 (2006).
7. N. Engheta, "Circuits with Light at Nanoscales: Optical Nanocircuits Inspired by Metamaterials," Science **317**, 1698-1702 (2007).
8. D. Schurig, J. J. Mock, B. J. Justice, S. A. Cummer, J. B. Pendry, A. F. Starr, and D. R. Smith, "Metamaterial electromagnetic cloak at microwave frequencies," Science **314**, 997-980 (2006).
9. A. Alu and N. Engheta, "Achieving transparency with plasmonic and metamaterial coatings," Phys. Rev. E **72**, 016623 (2005).
10. R. A. Shelby, D. R. Smith, and S. Schultz, "Experimental Verification of a Negative Index of Refraction," Science **292**, 77-79 (2001).

#102228 - $15.00 USD Received 2 Oct 2008; revised 30 Oct 2008; accepted 31 Oct 2008; published 3 Nov 2008

11. V. M. Shalaev, "Optical negative-index metamaterials," Nature Photon. **1**, 41-48 (2007) and references therein.
12. A. Alu, A. Salandrino, and N. Engheta, "Negative effective permeability and left-handed materials at optical frequencies," Opt. Express **14**, 1557-1567 (2006).
13. J. Valentine, S. Zhang, T. Zentgraf, E. Ulin-Avila, D. A. Genov, G. Bartal, and X. Zhang, "Three-dimensional optical metamaterial with a negative refractive index," Nature **455**, 376-379 (2008).
14. H. T. Miyazaki and Y. Kurokawa, "Squeezing visible light waves into a 3-nm-thick and 55-nm-long plasmon cavity," Phys. Rev. Lett. **97**, 097401 (2006)
15. E. Verhagen, J. A. Dionne, L. (Kobus) Kuipers, H. A. Atwater, and A. Polman, "Near-field visualization of strongly confined surface plasmon polaritons in metal-insulator-metal waveguides," Nano Lett. **8**, 2925-2929 (2008)
16. H. Shin and S. Fan, "All-angle negative refraction for surface plasmon waves using a metal-dielectric-metal structure," Phys. Rev. Lett. **96**, 073907 (2006)
17. G. Shvets, "Photonic approach to making a material with a negative index of refraction," Phys. Rev. B. **67**, 035109 (2003)
18. M. Stockman, "Criteria for negative refraction with low optical losses from a fundamental principle of causality," Phys. Rev. Lett. **98**, 177404 (2007)
19. A. Karalis, E. Lidorikis, M. Ibenescu, J. D. Joannopoulos, and M. Soljačić, "Surface-plasmon-assisted guiding of broadband slow and subwavelength light in air," Phys. Rev. Lett. **95**, 063901 (2005).
20. X. Fan, G. P. Wang, J. C. W. Lee, and C. T. Chan, "All-angle broadband negative refraction of metal waveguide arrays in the visible range: Theoretical analysis and numerical demonstration," Phys. Rev. Lett. **97**, 073901 (2006)
21. H. J. Lezec, J. A. Dionne, and H. A. Atwater, "Negative Refraction at Visible Frequencies," Science **316**, 430-432 (2007).
22. I. I. Smolyaninov, Y.-J. Hung, and C. C. Davis, "Magnifying Superlens in the Visible Frequency Range," Science **316**, 1699-1701 (2007).
23. A. S. Barker and R. Loudon, "Response functions in the theory of Raman scattering by vibrational and polariton modes in dielectric crystals," Rev. Mod. Phys. **44**, 18-47 (1972).
24. V. G. Veselago, "Electrodynamics of Substances with Simultaneously Negative Values of Sigma and Mu," Soviet Physics Uspekhi-Ussr **10**, 509-514 (1968).
25. M. Stockman, "Slow propagation, anomalous absorption, and total external reflection of surface plasmon polaritons in nanolayer systems," Nano Lett. **6**, 2604-2608 (2006).
26. R. Ruppin, "Electromagnetic energy density in a dispersive and absorptive material," Phys. Lett. A **299**, 309-312 (2002).
27. P. B. Johnson and R. W. Christy, "Optical constants of the noble metals," Phys. Rev. B **6**, 4370-4379 (1972)
28. *Handbook of Optical Constants of Solids*, edited by E. Palik (Academic Press, Inc., New York, 1985).
29. Lumerical FDTD Solutions 6.0

1. Introduction

The interaction of light with matter is almost exclusively determined by the electric permittivity ε and magnetic permeability μ, two intrinsic material properties that describe the response of charges and currents to an applied electromagnetic field. At optical frequencies, both the permittivity and the permeability of all transparent natural materials are positive, leading to a positive index of refraction. However, if the sign and magnitude of the index could be tuned at will, the flow of light could be controlled in unprecedented ways [1,2]. Among the many unusual applications of index tunability are sub-diffraction-limited superlenses [3-6], optical nanocircuits [7], and cloaks to render objects invisible [8,9].

In recent years, metamaterials have received considerable attention for their ability to precisely control the dispersion and propagation of light. These engineered materials are generally composed of subwavelength resonators – such as metallic coils or rods – that serve as 'artificial' atoms of the material [10-12]. Considered as a bulk material, these metamaterials will exhibit properties altogether distinct from their constituent resonator elements. Through variation of the resonator materials or dimensions, metamaterials allow for refractive index tunability that can span positive, negative, and near-zero indices. Resonator-based metamaterials have been shown to effectively cloak two-dimensional objects at microwave frequencies [8], and have recently exhibited negative refraction at infrared frequencies [13].

#102228 - $15.00 USD Received 2 Oct 2008; revised 30 Oct 2008; accepted 31 Oct 2008; published 3 Nov 2008

Apart from resonator-based metamaterials, surface-plasmon-based geometries have also been shown to exhibit broad index tunability [14, 15]. Unlike traditional metamaterials, these geometries consist of planar waveguides with alternating layers of metals and dielectrics. Light propagates through the structure via one or more surface plasmon waves, which are characterized by group and phase velocities distinct from the incident light. If the waveguide is characterized by only a single propagating mode, light will emerge from the structure as if it had passed through a material with an index equal to the mode index. Such plasmon-based geometries have the potential to exhibit the same response as resonator-based metamaterials [12, 16-19], without the necessity of patterning discrete resonator elements. Of course, single slab waveguides will exhibit an anisotropic response, restricting guided wave propagation to two dimensions. This characteristic renders planar waveguides particularly useful for on-chip applications, where optical components are interconnected in-plane. However, plasmonic waveguides can also potentially serve as basic elements of fully three-dimensional metamaterials, when arranged in stacked geometries [17, 20].

Experimentally, negative refraction at visible frequencies has been directly observed in metal-insulator-metal (MIM) surface plasmon waveguides [21]. In addition, superlensing has been reported for plasmonic waveguides coated with a thin insulating layer (an insulator-insulator-metal, or IIM geometry) [22]. Still, debate remains as to whether these structures exhibit the requisite condition of negative index materials: namely, light propagation characterized by oppositely-oriented phase and energy velocities. Moreover, the attainable mode indices and propagation lengths, as well as constraints on geometrical parameters, remain largely unexplored.

In this paper, we theoretically investigate the range of negative and positive indices accessible in these surface plasmon waveguides, including calculations of dispersion and absorption. Attention is given to the modes of MIM, IIM, and insulator-metal-insulator (IMI) waveguides. Our analysis considers both Ag/Si_3N_4 and Ag/GaP - based geometries, to compare the effect of different insulator permittivities. We vary the core waveguide dimensions from 5 nm to 50 nm in 1 nm increments and the excitation wavelength from the ultraviolet to near-infrared. By carefully exploring the magnitude and sign of complex wavevectors accessible in these structures, we explicitly determine their utility as negative index materials. Our analytic results are confirmed with finite difference time domain simulations that directly demonstrate the refraction of free-space waves into these plasmonic materials. In addition, our analysis provides detailed maps of plasmonic indices and figures of merit as a function of wavelength and geometry. Such maps serve as a "guide to the experimentalist" in designing future plasmon-based negative index materials and transformation-based (i.e., index-tuned) optical elements.

2. Theoretical formalism

In conventional materials, the complex refractive index can be derived from knowledge of the wavelength and absorption of light in the material. Surface-plasmon-based geometries are no exception. The plasmon wavevector k_x can be used to uniquely determine the complex refractive index of waves traveling along a direction x parallel to a metallo-dielectric interface. A dispersion relation relates the wavevector k_x and frequency ω, which are both in general complex quantities [23]. However, in the context of monochromatic excitation of a waveguided mode, it is sensible to impose the frequency to be real. The complex wavevector then describes spatial propagation and decay of the surface plasmon wave along the waveguide. This mode's wavelength λ_{SP} and index n are related to the magnitude of the real component of k_x via

$$\lambda_{SP} = 2\pi \Big/ |\,\mathrm{Re}\{k_x\}\,| \qquad \text{and} \qquad n = c \cdot \mathrm{Re}\{k_x\} \Big/ \omega . \tag{1}$$

The extinction of the wave can be extracted from the magnitude of the imaginary component of k_x, with mode propagation lengths L_{SP} given by:

#102228 - $15.00 USD Received 2 Oct 2008; revised 30 Oct 2008; accepted 31 Oct 2008; published 3 Nov 2008

$$L_{SP} = 1/2 \cdot \mathrm{Im}\{k_x\}. \quad (2)$$

Solving Maxwell's equations subject to continuity of the tangential electric fields and normal displacement fields yields the wavevector. Assuming wave propagation along the positive *x*-direction, surface plasmons take the form of transverse-magnetic waves:

$$E(x,z,t) = (E_x \hat{x} + E_z \hat{z}) e^{i(k_x x - \omega t)} \quad (3)$$

$$H(x,z,t) = (H_y \hat{y}) e^{i(k_x x - \omega t)}. \quad (4)$$

For a three-layered geometry with each interface parallel to *x* and perpendicular to *z* (see inset of Fig. 1(a)), the electric field components of each j^{th} layer may be written as:

$$E_{xj} = a_j e^{k_{zj} z} + b_j e^{-k_{zj} z} \quad (5)$$

$$E_{zj} = \left(\frac{ik_x}{k_{zj}}\right)\left(-a_j e^{k_{zj} z} + b_j e^{-k_{zj} z}\right), \quad (6)$$

with k_{zj} defined by momentum conservation:

$$k_{z0,1,2}^2 = k_x^2 - \varepsilon_{0,1,2}\left(\frac{\omega}{c}\right)^2. \quad (7)$$

The in-plane wavevector k_x is then determined by applying the boundary conditions at each interface. The determinant of the coefficients a_j and b_j yields the dispersion relationship connecting k_x and ω:

$$\det\left(\begin{bmatrix} 0 & 1 & 0 & 0 & 0 & 0 \\ 1 & 1 & -1 & -1 & 0 & 0 \\ -\frac{\varepsilon_0}{k_{z0}} & \frac{\varepsilon_0}{k_{z0}} & \frac{\varepsilon_1}{k_{z1}} & -\frac{\varepsilon_1}{k_{z1}} & 0 & 0 \\ 0 & 0 & e^{k_{z1}d_1} & e^{-k_{z1}d_1} & -e^{k_{z2}d_1} & -e^{-k_{z2}d_1} \\ 0 & 0 & -\frac{\varepsilon_1}{k_{z1}} e^{k_{z1}d_1} & \frac{\varepsilon_1}{k_{z1}} e^{-k_{z1}d_1} & \frac{\varepsilon_2}{k_{z2}} e^{k_{z2}d_1} & -\frac{\varepsilon_2}{k_{z2}} e^{-k_{z2}d_1} \\ 0 & 0 & 0 & 0 & 1 & 0 \end{bmatrix}\right) = 0 \quad (8)$$

Note that the waveguide is assumed to be infinite in the *y* direction. Each layer {0,1,2} is described by either a real or complex electric permittivity $\varepsilon_{0,1,2}$ and a thickness *d*, with d_0 and d_2 assumed to be semi-infinite. All materials are considered linear and non-magnetic, with the magnetic permeability $\mu = 1$. Roots of the dispersion relation are found in the complex k_x plane by a minimization algorithm.

It is well known that light propagation in isotropic negative index materials is characterized by antiparallel phase and energy flow [24]. For all propagating plane waves (with $\mathrm{Real}\{k_x\} \neq 0$), the phase velocity is defined by $v_p = \omega/\mathrm{Real}\{k_x\}$. In the absence of losses and high dispersion, the energy velocity v_E is equal to the group velocity $v_g = d\omega/dk_x$. Therefore, for lossless materials, negative indices will manifest themselves by a region of negative slope on a plot of ω versus $|k_x|$.

#102228 - $15.00 USD Received 2 Oct 2008; revised 30 Oct 2008; accepted 31 Oct 2008; published 3 Nov 2008

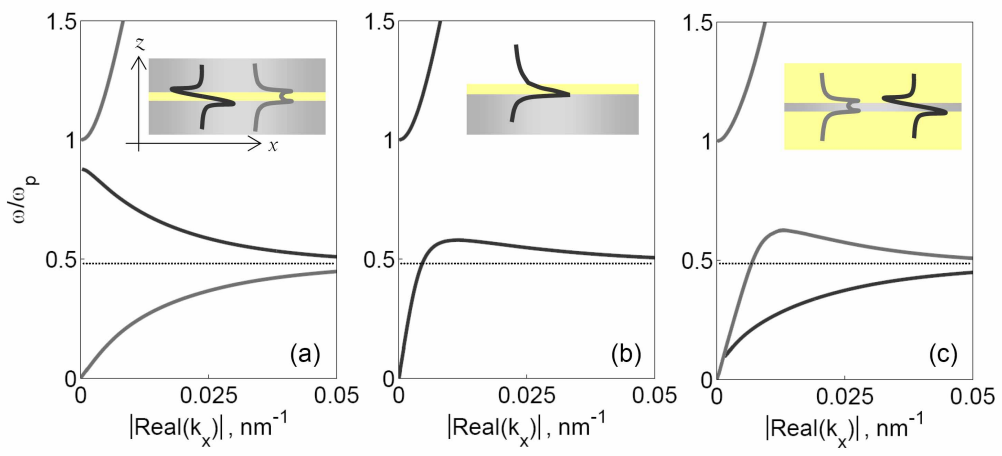

Fig. 1. Lossless dispersion for three plasmon geometries: (a) a MIM waveguide composed of 50 nm GaP clad by Ag; (b) an IIM waveguide composed of a semi-infinite Ag film coated with 20 nm GaP; and (c) an IMI waveguide composed of 50 nm Ag clad by GaP. The dotted line indicates ω_{SP}. Insets show the waveguide geometry and the associated H_y mode profiles for both the symmetric mode (light gray) and the antisymmetric mode (dark gray). Notice that all three geometries are characterized by regions of negative slope and hence negative indices. However, this negative index regime is single valued in k_x for the MIM geometry only.

Figure 1 plots the dispersion relationships ω versus |Real{k_x}| for *lossless* MIM, IIM, and IMI geometries with Ag as the metallic layer and GaP as the dielectric. Here, the Ag is described by a lossless Drude model with a bulk plasma frequency $\hbar\omega$ = 9.01 eV. The index of GaP is taken as 3.31. For reference, the surface plasmon resonance frequency is shown as a dotted line. In Fig. 1(a), 50 nm of GaP is surrounded by two semi-infinite layers of Ag. As seen, the dispersion curve of this MIM geometry is characterized by three distinct bands, including a region of negative slope between the bulk and surface plasmon frequencies and regions of positive slope below the surface plasmon resonance and above the bulk plasma resonance. Note that these three bands correspond to two different modes with varying magnetic field distributions across the waveguide. Below the surface plasmon resonance, $H_y = B/\mu$ is symmetric across the waveguide (light gray branch). The wavevectors of this mode are purely real below the surface plasmon resonance, but become purely imaginary for frequencies between the bulk and surface plasmon resonance frequencies. In contrast, H_y is antisymmetric throughout the regime of negative slope (dark gray branch). Interestingly, the wavevectors of this antisymmetric mode become purely imaginary for frequencies below the surface plasmon resonance. Thus, the MIM modes allowed to propagate in the traditional surface plasmon bandgap (between the bulk and surface plasmon resonant frequencies) have a field distribution altogether distinct from the propagating plasmon modes below resonance.

As seen in Fig. 1(a), each input frequency is assigned to a unique MIM wavevector throughout the entire *k*-space domain. Therefore, for a given excitation wavelength, this lossless MIM geometry will be characterized by a single propagating mode. Provided excitation wavelengths are between the bulk and surface plasmon resonance frequencies, the plasmon mode will exhibit a negative index, rendering the entire MIM composite an effective negative index material.

Like the lossless MIM geometry, IIM and IMI waveguides are also characterized by regions of negative slope, and hence negative indices. For example, Fig. 1(b) plots the dispersion relationship for the bound modes of a semi-infinite layer of Ag coated with a thin, 20 nm thick layer of GaP. As seen, this geometry is characterized by a single continuous bound mode for frequencies below and above the surface plasmon resonance. Its dispersion follows that of surface plasmons at a single Ag/air interface for low frequencies and wavevectors, but as a larger fraction of the field is contained in the GaP for higher

#102228 - $15.00 USD Received 2 Oct 2008; revised 30 Oct 2008; accepted 31 Oct 2008; published 3 Nov 2008

frequencies, the wavevector diverges at the Ag/GaP surface plasmon resonance. For frequencies above the surface plasmon resonance, this mode can exhibit negative slope, corresponding to oppositely-oriented group and phase velocities. Note, however, that this geometry is not characterized by a unique wavevector assignment at each frequency. Above the surface plasmon resonance, for example, this lossless IIM geometry is characterized by two wavevectors, and hence two propagating waves of different wavelength. Since each excitable wavevector resides in regimes of opposite slope, these two waves will be characterized by counter-propagating phase. Note, however, that a frequency regime with double wavevector solutions exists only for insulator thicknesses smaller than a critical cutoff thickness [25].

Similar features can be observed for the bound modes of the IMI geometry, plotted in Fig. 1(c). Here, 50 nm of Ag is clad by two semi-infinite regions of GaP. Like the MIM geometry, this structure is characterized by both a H_y-field anti-symmetric mode (light gray curve, located exclusively below the surface plasmon resonance) and a H_y-symmetric mode (dark gray, located both above and below the surface plasmon resonance). The symmetric mode exhibits a regime of negative slope for certain frequencies above the plasmon resonance frequency. However, as with the IIM geometry, this negative index regime is accompanied by wavevectors that exhibit positive slope – and hence a positive index – throughout the same frequency range.

As Fig. 1 reveals, in the absence of losses all three plasmonic geometries appear to support propagation of negative index modes over a finite frequency range. However, the MIM geometry is the only structure that can be characterized by a single propagating negative index mode – and hence a unique negative index – for these frequencies. Of course, the many enabling and exotic applications of plasmonic systems, including negative indices, do not come without an expense: namely, the cost of losses. Metals are characteristically lossy, particularly near their resonant frequencies, and Ag is no exception. While this section outlined the potential for plasmon waveguides to support propagation of negative index waves, the next section explores the extent to which these results are altered when losses are included.

3. Lossy dispersion and the necessary condition for negative indices

The equivalence between the energy velocity v_E and the group velocity v_g described above provides a simple way of identifying negative index regimes directly from a dispersion diagram. However, this equivalence only holds for non-absorbing media. For absorbing (i.e., lossy) materials, the more general expression of the energy velocity must be used:

$$v_E = S/W \tag{9}$$

where S is the average power flow in the waveguide and W is the time-averaged energy density [26]. The average power flow can be derived from the integrated Poynting flux, and always points in the direction of wave propagation. Therefore, the direction of power flow will be collinear with the direction of wave decay for lossy materials:

$$\text{sign}(v_E) = \text{sign}(\text{Imag}\{k_x\}). \tag{10}$$

In contrast to power flow, phase can flow in either direction, either parallel or opposite to the direction of wave decay. For plane waves, including plasmons, phase flow is described by the ratio of the excitation frequency to the mode wavevector via $v_p = \omega/\text{Real}\{k_x\}$ and so:

$$\text{sign}(v_p) = \text{sign}(\text{Real}\{k_x\}). \tag{11}$$

Therefore, to achieve the antiparallel energy and phase velocities associated with negative indices, the plasmon wavevector must satisfy the criteria:

#102228 - $15.00 USD Received 2 Oct 2008; revised 30 Oct 2008; accepted 31 Oct 2008; published 3 Nov 2008

$$\text{sign}(\text{Real}\{k_x\}) \neq \text{sign}(\text{Imag}\{k_x\}), \tag{12}$$

assuming the electromagnetic fields take the form $e^{i(k_x x-\omega t)}$. Note that this condition on the sign of the real and imaginary components of k is both a necessary and sufficient condition for achieving negative indices in absorbing media, including plasmon-based geometries [25].

Because of point symmetry in the complex k_x plane with respect to the origin, we can impose $\text{sign}(\text{Imag}\{k_x\}) \geq 0$. This choice restricts the direction of net energy flow to the positive x direction. Then, negative index plasmonic geometries will necessarily be characterized by a negative real component of the plasmon wavevector. Assuring consistency with Fig. 1, we note that the choice of $\text{sign}(\text{Imag}\{k_x\}) \geq 0$ also affects the sign of $\text{Real}\{k_x\}$ obtained in the lossless dispersion curves. Notably, the branches plotted in Fig. 1 are accompanied by counterpropagating modes that have $k_x < 0$. Imposing a constraint on the energy flow direction allows only curves with positive slope in the lossless case. The branches with negative slope in Fig. 1 (which were recognized as exhibiting a negative index) are then omitted. Instead, their counterparts with $k_x < 0$ remain, reflecting the connection between the signs of k_x and n when imposing this restriction on the direction of energy flow. As we will see, these dispersion curves can still be recognized when realistic material parameters, including absorption losses, are used.

3.1 The metal-insulator-metal waveguide as a negative index material

Figure 2 plots the real and imaginary components of the plasmon wavevector k_x versus energy for MIM geometries. Here, the metallic layer is Ag, described by the empirically-determined optical constants reported in Johnson and Christy [27]. The insulating layer is again taken to be GaP, with absorption both above and below the bandgap included [28]. GaP core thicknesses of 10 nm, 17 nm, and 25 nm are considered. For reference, the surface plasmon resonance is shown as a dotted horizontal line. As noted in Fig. 1(a), MIM geometries are characterized by both a H_y field symmetric mode and a H_y field antisymmetric mode. Both

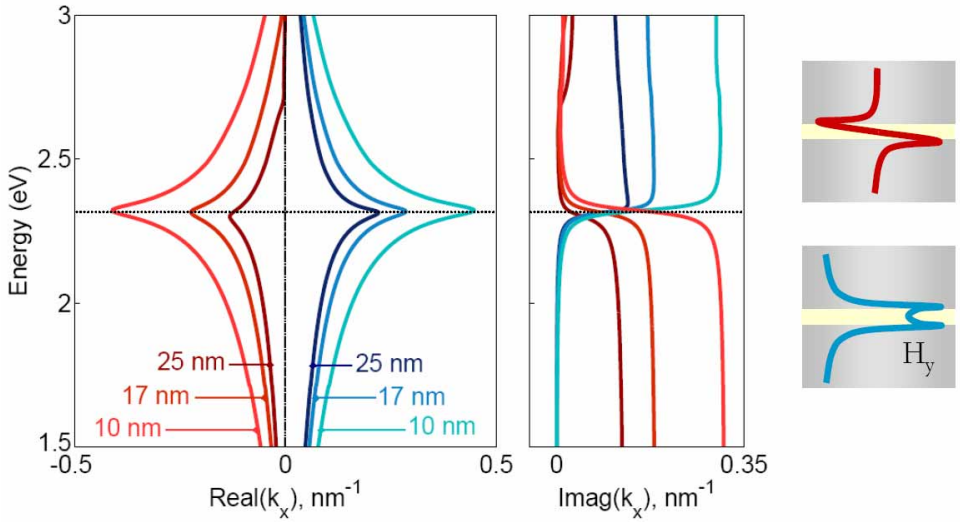

Fig. 2. Lossy dispersion for MIM waveguides consisting of GaP clad by Ag. Three GaP thicknesses are included (d = 25 nm, 17 nm, and 10 nm), and dispersion relations for both H_y-field symmetric (blue hues) and antisymmetric (red hues) modes are shown. Including losses, the necessary condition for negative index modes is: $\text{sign}(\text{Real}\{k_x\}) \neq \text{sign}(\text{Imag}\{k_x\})$. This condition is clearly satisfied for the H_y-field antisymmetric mode, which can exhibit negative indices with very low loss above the surface plasmon resonance (shown as a dotted line).

#102228 - $15.00 USD Received 2 Oct 2008; revised 30 Oct 2008; accepted 31 Oct 2008; published 3 Nov 2008

modes are also found in this lossy geometry, with the H_y-symmetric mode (with Real$\{k_x\} > 0$) shown in blue and the H_y-antisymmetric mode (with Real$\{k_x\} < 0$) plotted in red. Schematics of these mode profiles are also plotted in Fig. 2.

As seen in Fig. 2, the losses of the H_y-symmetric mode are quite low below the surface plasmon resonance frequency. Recall that between the surface plasmon and bulk plasma frequencies, this mode exhibited a bandgap in the lossless case, where k_x was purely imaginary. The introduction of loss now causes the real component to be non-zero in this frequency regime as well. However, since Imag$\{k_x\} >>$ Real$\{k_x\}$ above the surface plasmon resonance, the mode is in essence still a nonpropagating evanescent wave. Importantly, although this mode exhibits a regime of negative slope in the plot of Real$\{k_x\}$, its real wavevector component, and hence the phase velocity, remains exclusively positive. Since Imag$\{k_x\} > 0$, both energy velocity and phase velocity of the mode are always positive. Accordingly, these H_y-symmetric modes will be characterized by refractive indices that are exclusively positive throughout all frequencies.

While the H_y-symmetric modes do not exhibit negative indices, MIM waveguides can also support H_y-antisymmetric modes. The real and imaginary wavevector components of these modes are shown in Fig. 2 in red. As seen, the sign of Real$\{k_x\}$ is negative throughout the entire frequency domain, corresponding to a negative phase velocity. In contrast, the sign of Imag$\{k_x\}$ is positive. Therefore, these antisymmetric modes will exhibit oppositely-oriented energy and phase velocities, and hence negative indices. Note that Imag$\{k_x\} >>$ Real$\{k_x\}$ for frequencies below the surface plasmon resonance, indicating that these modes are essentially non-propagating below resonance. Such results are consistent with the lossless dispersion curves of Fig. 1(a), where the wavevector of the antisymmetric mode was purely imaginary below the surface plasmon resonance. However, above resonance, the losses of this H_y-antisymmetric mode become remarkably low – so low, in fact, that losses begin rival the low Imag$\{k_x\}$ components seen for the propagating positive index mode. The low losses reflect the allowed band of propagation for this mode seen in Fig. 1(a). Therefore, between the bulk and surface plasmon resonant frequencies, the H_y-antisymmetric mode will be the only propagating mode. As this mode exhibits opposite phase and energy velocities, MIM

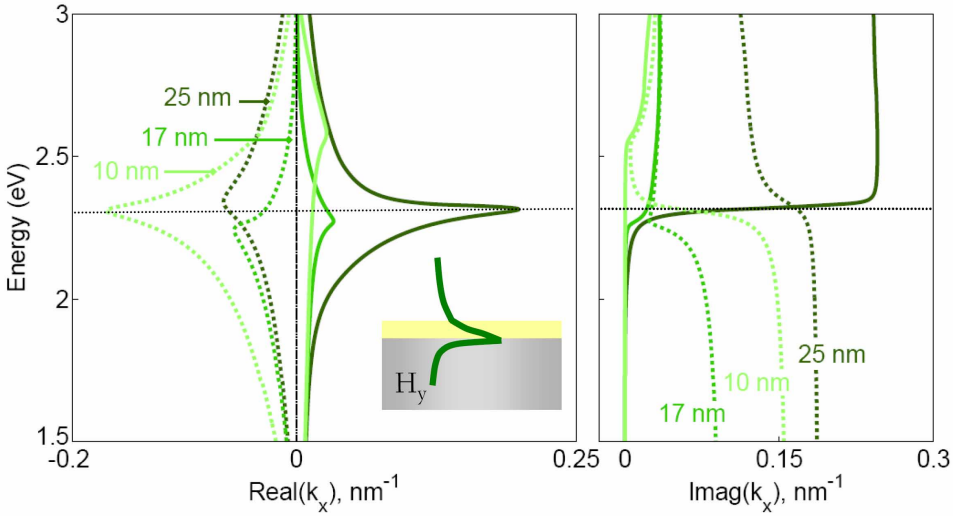

Fig. 3. Lossy dispersion for insulator-insulator-metal waveguides composed of a semi-infinite Ag film coated with a thin layer of GaP and embedded in air. Three GaP thicknesses are included (d = 25 nm, 17 nm, and 10 nm), and dispersion relations for both positive index (solid) and negative index (dotted) branches are shown. While solutions satisfying sign(Real$\{k_x\}$) ≠ sign(Imag$\{k_x\}$) may be found, the losses are quite high, with propagation lengths comparable to or smaller than the mode wavelength.

#102228 - $15.00 USD Received 2 Oct 2008; revised 30 Oct 2008; accepted 31 Oct 2008; published 3 Nov 2008

geometries will indeed be characterized by negative indices in this frequency range. The range of achievable refractive indices and figures of merit (Real{k_x}/Imag{k_x}) will be discussed in detail in Section 4.

3.2 Insulator-insulator-metal and insulator-metal-insulator waveguides as multimode metamaterials

Figure 3 plots the dispersion relationship for the bound modes of an IIM waveguide, considering both the sign and magnitude of Real{k_x} and Imag{k_x}. A thick Ag slab is coated with a thin layer of GaP (d = 10 nm, 17 nm, and 25 nm) and embedded in air. The dielectric functions of Ag and GaP are adopted from empirically-determined optical constants, and thus include realistic losses for all plotted frequencies. As with the MIM waveguides, this geometry exhibits real wavevector components that are both positive and negative, corresponding to positive and negative indices, respectively. Below resonance, only the positive index mode exhibits long-range propagation. Above resonance, the losses of this positive index mode increase, while the losses of the negative index mode are reduced. Note however that unlike the MIM geometry, the losses of the IIM negative index mode are generally comparable with those of the positive index mode. For example, GaP thicknesses of 10 nm and 17 nm exhibit negative-index Imag{k_x} components that are higher than for the positive index mode. As the thickness of GaP is increased to 25 nm, the losses of both modes increase dramatically. This increased loss reflects the presence of the cutoff thickness for the negative index mode. For thicker dielectrics both modes exhibit very short propagation lengths above the surface plasmon resonance frequency that are comparable to or smaller than the mode wavelength.

Similar features are observed for the H_y-symmetric mode of an IMI waveguide, shown in Fig. 4. Recall that this mode exhibited simultaneously positive and negative indices above the surface plasmon resonance for the lossless geometry (Fig. 1(c)). Here, a thin Ag slab is embedded in GaP. Ag thicknesses of d = 10 nm, 17 nm, and 25 nm are considered. Note that the wavevectors of the H_y-antisymmetric mode are not shown, since this mode is characterized by exclusively positive wavevectors with Imag{k_x} components that generally

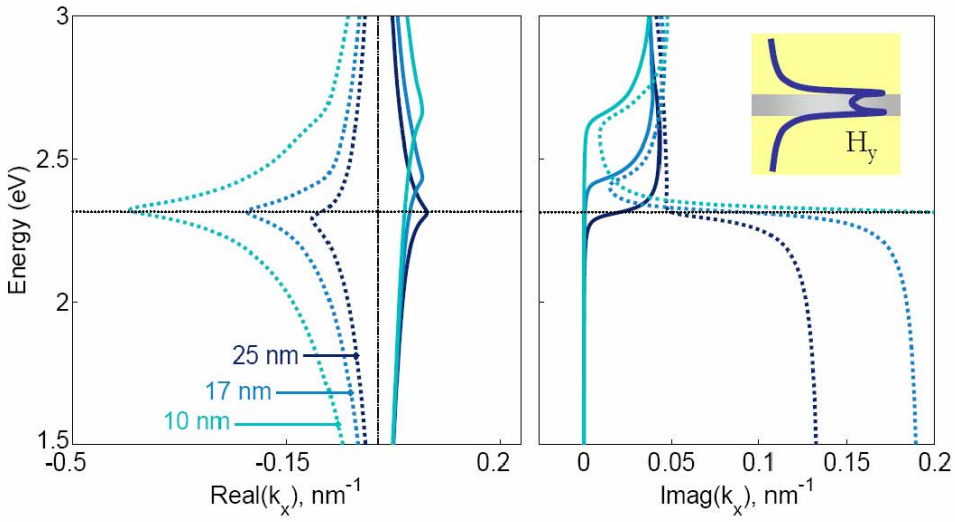

Fig. 4. Lossy dispersion for insulator-metal-insulator waveguides composed of a thin Ag film clad with GaP. Three Ag thicknesses are included (d = 25 nm, 17 nm, and 10 nm), and dispersion relations for the positive and negative index branches of the H_y-field symmetric mode are shown. While solutions satisfying sign(Real{k_x}) ≠ sign(Imag{k_x}) may be again found, the losses of this branch always exceed those of the positive index mode.

#102228 - $15.00 USD Received 2 Oct 2008; revised 30 Oct 2008; accepted 31 Oct 2008; published 3 Nov 2008

exceed those of the symmetric mode. As with the MIM and IIM geometries, losses for the positive index IMI modes are low below resonance, but increase strongly in the bandgap region. In contrast, losses for the negative index mode are high below resonance, and can be substantially reduced above resonance. However, the losses for these negative index modes are generally *never* lower than the losses for the positive index modes.

As Figs. 3 and 4 reveal, both IIM and IMI geometries can support negative index modes. However, these negative index modes are generally found in a frequency regime where additional positive index modes also exist. Such characteristics prohibit assignment of a single, unique index to the IIM and IMI geometries above the plasmon resonance, even including realistic material losses. Therefore, unlike the MIM geometry, planar IIM and IMI waveguides may not be regarded as single-mode, negative index materials. Nevertheless, the existence of multiple modes propagating with opposite phase and comparable absorption may be interesting for a variety of on-chip photonic applications. Moreover, their symmetric mode profiles may render these waves more easily excitable than the asymmetric negative index modes of MIM geometries.

4. Mapping plasmonic material indices and figures of merit: A guide to the experimentalist

Design of practical metamaterials requires precise knowledge of the index and absorption. For plasmonic geometries, such parameters strongly depend on the constituent materials, the structure dimensions, and the excitation wavelength. The preceding sections outlined the

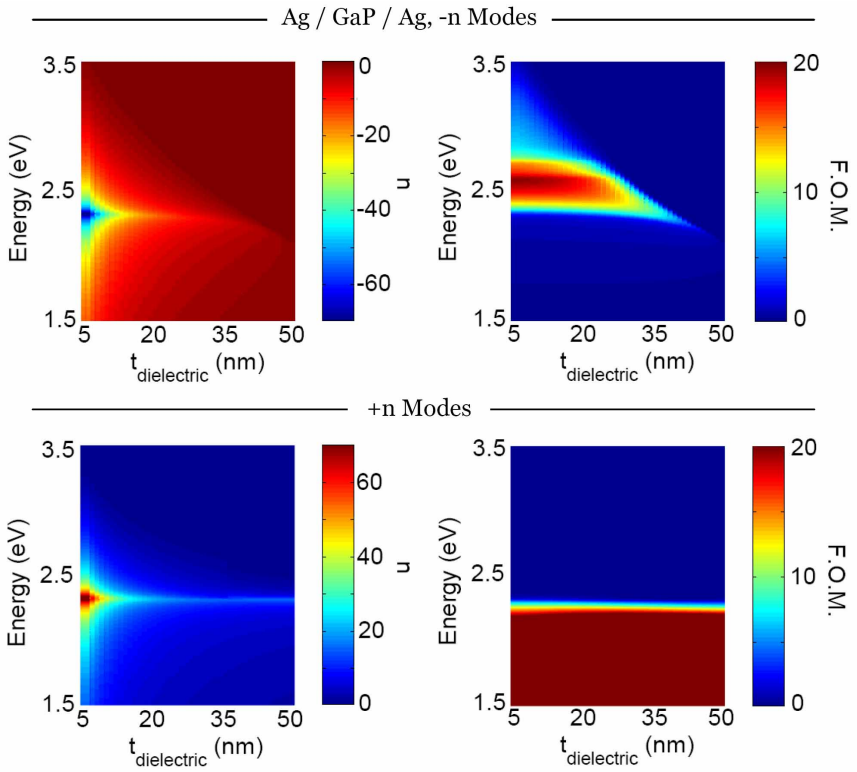

Fig. 5. Plots of MIM indices and figures of merit (FOM) for Ag/GaP/Ag waveguides as a function of energy and core thickness. Maps for both positive and negative index modes are shown. While the FOM for positive index modes drops to zero above the plasmon resonance frequency, it can be as high as 20 above resonance for negative index modes.

#102228 - $15.00 USD Received 2 Oct 2008; revised 30 Oct 2008; accepted 31 Oct 2008; published 3 Nov 2008

potential for vast index tunability in plasmonic waveguides: while MIM geometries can achieve low-loss, single-mode negative indices above the plasmon resonance, IIM and IMI geometries can sustain simultaneous propagation of waves with positive and negative phase. In addition, the magnitude of the wavevectors (and hence the mode indices) can span from near-zero to large positive and negative values. In this section, we explore the range of achievable indices and figures of merit in plasmonic waveguides. The associated plots are intended as a guide to the experimentalist in designing plasmonic materials for a variety of metamaterial and transformation-based applications.

4.1 Ag/GaP and Ag/Si_3N_4 MIM metamaterials: Negative indices and negative refraction

Figure 5 plots the achievable refractive indices and figures of merit for MIM geometries, using GaP as the core and Ag as the cladding. Here, the figure of merit (FOM) is defined as the magnitude of the ratio of Real{k_x} to Imag{k_x}, or equivalently, Real{n} to Imag{n}. GaP core thicknesses are varied from 5 nm to 50 nm in 1 nm increments, and excitation wavelengths are varied from the near-infrared to the ultraviolet (energies of 1.5 – 3.5 eV). Note that each vertical cut through the chart depicts one dispersion diagram, with the index and FOM plotted on the color scale. Index maps are provided for both the negative and positive index modes.

As seen in the figure, both modes achieve refractive index magnitudes spanning from $|n| \approx 0$ to $|n| > 60$ as the core GaP thickness is reduced. As expected, figures of merit for the negative index mode are near zero for frequencies below the surface plasmon resonance, but approach 20 for thinner waveguides excited above resonance. Interestingly, these figures of merit can be orders of magnitude higher than the FOM for positive index modes above resonance. Moreover, the FOM for the negative index modes actually increases with decreasing core thickness. For example at a wavelength of ~480 nm (2.57 eV), negative indices of $n = -23$ can be achieved with figures of merit equal to 19.7, using a 5 nm thick GaP core. In contrast, the FOM for the positive index mode at the same wavelength is smaller than 0.5. Note, however, that the increasing FOM with decreasing core thickness does not necessarily imply an increase of the propagation length, as n becomes larger as well.

To investigate the refraction of light into such a negative index MIM waveguide, we performed a three-dimensional finite-difference time-domain simulation [29] of the structure depicted in Fig. 6(a). A 488-nm plane wave of infinite extent is incident *from free space* on a

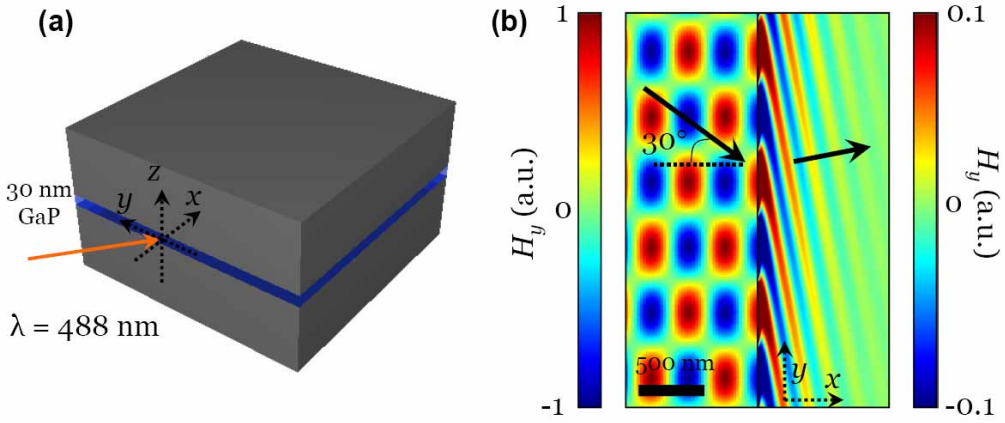

Fig. 6. Finite difference time domain simulation of negative refraction of a 488-nm plane wave into a MIM waveguide. (a) Schematic of the simulation geometry. The plane wave is incident at an angle of 30° with respect to the *xz* plane and 10° with respect to the *xy* plane. (b) H_y field component snapshot in a plane through the waveguide core. Bloch boundary conditions are used to simulate an incident plane wave that is infinite in extent. For clarity, the color scale in the waveguide to the right differs from that in the air region to the left. The arrows depict the calculated Poynting vector directions of the incident and refracted waves.

#102228 - $15.00 USD Received 2 Oct 2008; revised 30 Oct 2008; accepted 31 Oct 2008; published 3 Nov 2008

30-nm-thick GaP slot clad with 400nm Ag. At this wavelength, this geometry has a negative index of $n = -2.86$ with a figure of merit equal to 10. In order to allow excitation of the H_y-antisymmetric mode in the waveguide, the wave is polarized in the z direction and incident at a slightly oblique angle (10°) to the xy plane. Bloch boundary conditions are used to simulate an incident plane wave that is infinite in extent. Figure 6(b) shows the simulated H_y field in a plane through the waveguide core at a distance of 5 nm from the top Ag/GaP interface. To the left, the incident wave makes an angle of 30° with respect to the x axis, as shown by the arrow indicating the calculated Poynting vector. Inside the MIM waveguide, a wave can be seen to propagate over a micron-sized distance. The wave front angle is consistent with a negative index of $n = -2.86$, as predicted. Additionally, in the first 100 nm from the edge of the waveguide, the quickly decaying contribution of the largely evanescent H_y-symmetric mode can be recognized. By calculating the Poynting vector in the waveguide beyond the first 100 nm, power is seen to flow away from the normal in the direction associated with negative refraction. This result proves that the negative index mode can indeed enable negative refraction of light.

Replacing the GaP with Si_3N_4 ($n \sim 2.02$) shifts the surface plasmon resonance to higher energies. Figure 7 shows index and FOM maps for Ag/Si_3N_4/Ag MIM geometries, again with core thicknesses spanning 5 nm to 50 nm. As usual, the Ag and Si_3N_4 have been described by frequency-dependent dielectric constants adopted from the literature [21, 22]. As seen, the region of high figure of merit for negative index modes has increased in energy to 3.1 eV. While index magnitudes achievable in this geometry range are comparable with the GaP-based geometry, the maximum figure of merit has been reduced to 10. Heuristically, reducing

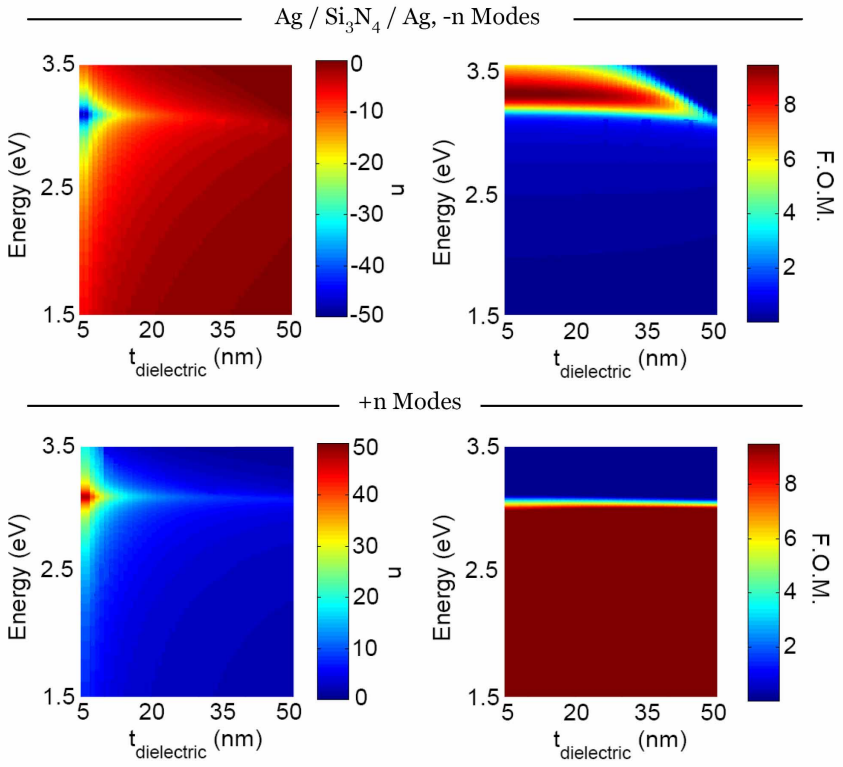

Fig. 7. Plots of MIM indices and figures of merit for Ag/Si_3N_4/Ag waveguides as a function of wavelength and core thickness. Maps for both positive and negative index modes are shown. The smaller index of Si_3N_4, compared with GaP, shifts the region of high FOM negative indices to shorter wavelengths, where Ag is more absorbing.

#102228 - $15.00 USD Received 2 Oct 2008; revised 30 Oct 2008; accepted 31 Oct 2008; published 3 Nov 2008

the dielectric index shifts the surface plasmon resonance towards the bulk plasma resonance, where Ag is inherently more absorbing. Nevertheless, the range of index tunability is significant: Not only are high figure-of-merit negative index materials achievable with MIM-based geometries, but these structures can also exhibit broadband operation. High FOM negative indices for this $Ag/Si_3N_4/Ag$ MIM geometry span wavelengths from 354 nm - 397 nm; in this wavelength range, FOMs range from 7-10. Likewise, high figure-of-merit negative indices for the Ag/GaP/Ag MIM geometry span wavelengths of 456 – 524 nm (energies of 2.37 – 2.72 eV) – a wavelength range of nearly 75 nm, where FOMs range from 12-20. Note that for higher energies, figures of merit for this GaP waveguide are predominately limited by increased absorption in the GaP.

4.2 Ag/GaP and Ag/Si_3N_4-based IIM and IMI Waveguides

Figure 8 plots the index and FOM maps for the bound modes of an IIM waveguide, considering a thick Ag slab coated with a thin layer of GaP and embedded in air. Figure 9 plots equivalent maps, but for a Ag slab coated with a thin layer of Si_3N_4. As before, the thicknesses of GaP and Si_3N_4 are varied from 5 nm to 50 nm in 1 nm increments. Similar to the results shown in Fig. 3, Figs. 8 and 9 reveal the existence of high FOM negative index modes. For thin insulating layers (d < 10 nm), the figures of merit for these modes can approach 16 and 7 for the GaP and Si_3N_4 geometries, respectively. However, regions of high negative-index FOM are generally accompanied by a positive index mode that has a large

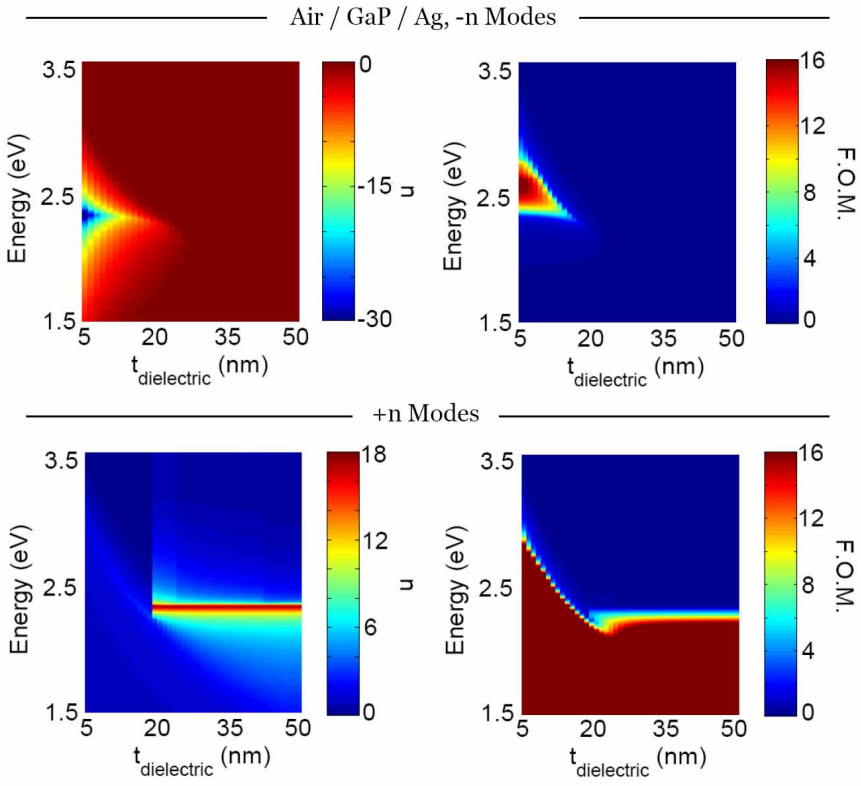

Fig. 8. Plots of IIM indices and figures of merit for Air/GaP/Ag geometries as a function of wavelength and core thickness. Both negative and positive index branches of the dispersion diagram are shown. While the negative index modes have a high figure of merit for small GaP thicknesses above the Ag/GaP plasmon resonance, the positive index modes also have a very high FOM there, too. Note that the abrupt change in index seen for d ~ 20 nm is related to the cutoff thickness of the negative index modes.

#102228 - $15.00 USD Received 2 Oct 2008; revised 30 Oct 2008; accepted 31 Oct 2008; published 3 Nov 2008

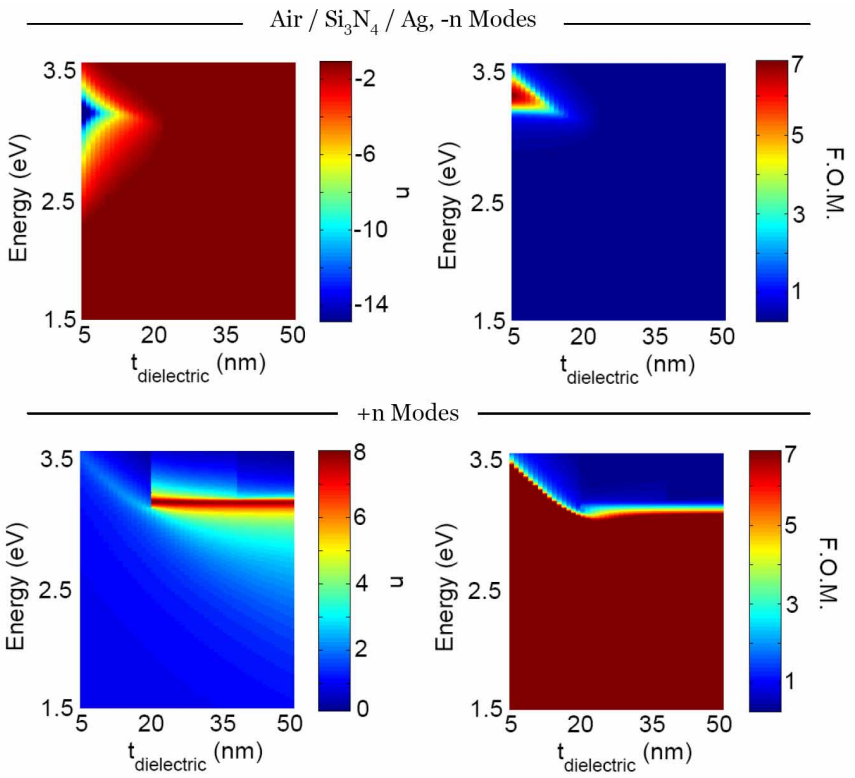

Fig. 9. Plots of IIM indices and figures of merit for Air/Si_3N_4/Ag geometries as a function of wavelength and core thickness. Both negative and positive index branches of the dispersion diagram are shown. As with the MIM geometries, the reduced index of Si_3N_4 shifts the region of high negative index FOM to shorter wavelengths. However, for this IIM geometry, the FOMs for the negative and positive index modes remain comparable in magnitude above the Ag/ Si_3N_4 plasmon resonance.

FOM as well. As seen in the bottom graphs of Figs. 8 and 9, the FOM for the positive index mode does not abruptly decay to zero above the Ag/GaP or Ag/Si_3N_4 surface plasmon resonance, as it did with the MIM-based geometries. Instead, as the dielectric thickness is decreased, the effective plasmon resonance increases towards the Ag/air surface plasmon frequency. Note that the abrupt change in index seen around d = 20 nm is related to the cutoff thickness of the negative index modes. Such results confirm the trends observed of Fig. 3: namely, that while IIM waveguides can support negative index modes, positive index modes with equally high figures of merit will also be present. Therefore, IIM geometries cannot be characterized as negative index materials identifiable with a unique index at a given wavelength.

Similar results are observed for IMI-based geometries, shown in Figs. 10 and 11 for GaP- and Si_3N_4-clad Ag slabs, respectively. For these waveguides, decreasing the thickness of Ag increases the FOM for both the positive and negative index modes. However, the FOM for the negative index modes never exceeds the FOM for the positive index modes. Indeed, as the Ag thickness is decreased, the electromagnetic field of this H_y-symmetric mode penetrates farther into the surrounding dielectric. For metallic slabs thinner than ~ 30 nm, the mode begins to approximate a plane wave traveling in a dielectric with an index equal to the cladding index. Therefore, even though negative index figures of merit can approach 18 and 10 for GaP and Si_3N_4-clad waveguides, respectively, the propagation of the traditional "long-ranging" positive index plasmon will generally dominate.

#102228 - $15.00 USD Received 2 Oct 2008; revised 30 Oct 2008; accepted 31 Oct 2008; published 3 Nov 2008

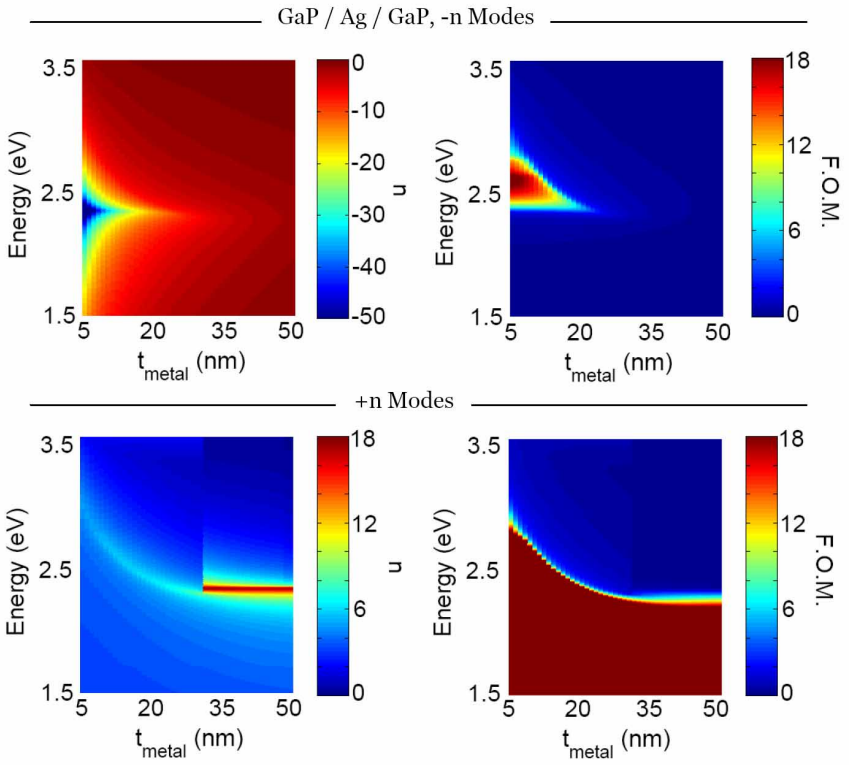

Fig. 10. Plots of IMI indices and figures of merit for GaP/Ag/GaP geometries as a function of wavelength and core thickness. Both negative and positive index branches of the dispersion diagram are included. Despite the large accessible negative indices, FOMs for this branch never exceed those of the positive index branch.

5. Conclusions

This paper has explored the range of positive and negative indices accessible in plasmonic geometries. Among planar plasmonic waveguides, MIM, IIM, and IMI-based structures all exhibit modes with negative indices between the bulk and surface plasmon resonances. Such negative index modes arise from an enhanced field penetration in the metal that gives rise to oppositely-oriented mode energy and phase velocities. Interestingly, these negative index modes can be characterized by high figures of merit despite high field confinement in the metal.

For MIM waveguides, the negative index mode is the only propagating (i.e., high figure-of-merit) mode between the bulk and surface plasmon resonances. In contrast, IIM and IMI waveguides support propagation of multiple high figure-of-merit modes, which are characterized by both positive and negative indices above resonance. Heuristically, the 'open' nature of these waveguides makes excitation and detection of IIM and IMI negative index modes inherently difficult, particularly since the negative and positive index modes share the same field symmetry. Therefore, IIM and IMI waveguides may not be formally considered metamaterials with a unique index assignment at a given frequency. However, they do provide an interesting platform for index tunability and multimode propagation, and their field symmetry makes them readily excitable by scattering or end-fire methods.

Unlike these "open" geometries, MIM waveguides are effective metamaterials that can be characterized by a unique index at each wavelength. For wavelengths below the surface plasmon resonance, the propagating plasmon mode is characterized by a symmetric H_y field

#102228 - $15.00 USD Received 2 Oct 2008; revised 30 Oct 2008; accepted 31 Oct 2008; published 3 Nov 2008

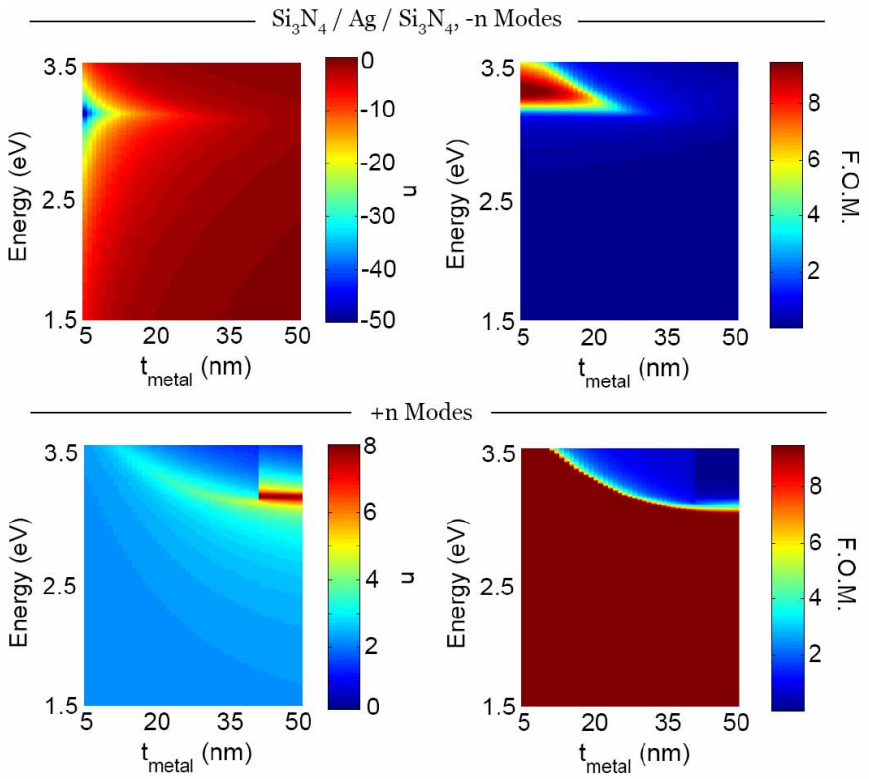

Fig. 11. Plots of IMI indices and figures of merit for $Si_3N_4/Ag/Si_3N_4$ as a function of wavelength and core thickness. The lower index of Si_3N_4shifts the plasmon resonance to shorter wavelengths, reducing the accessible FOM for both negative and positive index modes. However, as with GaP-based IMI waveguides, the FOM for the negative index modes never exceeds that of the positive index mode.

distribution and a positive index. Between the bulk and surface plasmon resonances, this symmetric mode becomes evanescent, rendering the antisymmetric H_y plasmon mode the only propagating mode. Interestingly, this antisymmetric mode is characterized by antiparallel energy and phase velocities, and hence negative indices. Therefore, light will propagate through the MIM waveguide as if through a negative index material, with an index equal to the plasmon mode index. Judicious choice of metal and dielectric can enable large negative indices with high figures of merit. For Ag/GaP geometries, such indices can range from 0 down to $n = -60$, with figures of merit approaching 20. Moreover, negative indices in MIM-based metamaterials can be achieved over a wide range of wavelengths (bandwidths of 75 nm are readily achievable) that are tunable throughout the entire visible spectrum. Note that efficient coupling and impedance matching into these waveguides requires excitation of an antisymmetric mode. Still, the broad index tunability of MIM waveguides, their high figures of merit, and their relative ease of fabrication may render MIM-based metamaterials an attractive alternative to resonator-based metematerials. Moreover, combined with traditional metamaterials, MIM geometries may enable realization of practical negative index and transformation-based optical elements, both in two-dimensional on-chip geometries and as basic elements of three-dimensional metamaterials.

Acknowledgments

The authors would like to thank A. F. Koenderink, L. Sweatlock, S. Burgos, H. J. Lezec, and L. (Kobas) Kuipers for engaging discussions related to this research. Work at Caltech is financially supported by the Department of Energy under grant DOE DE-FG02-07ER46405

#102228 - $15.00 USD Received 2 Oct 2008; revised 30 Oct 2008; accepted 31 Oct 2008; published 3 Nov 2008

and used facilities supported by the Center for Science and Engineering of Materials, an NSF MRSEC. Work at AMOLF is part of the Joint Solar Programme (JSP) of the Stichting voor Fundamenteel Onderzoek der Materie (FOM), which is financially supported by the Nederlandse organisatie voor Wetenschappelijk Onderzoek (NWO). The JSP is co-financed by gebied Chemische Wetenschappen of NWO and Stichting Shell Research. JAD gratefully acknowledges fellowship support from the National Science Foundation.

#102228 - $15.00 USD Received 2 Oct 2008; revised 30 Oct 2008; accepted 31 Oct 2008; published 3 Nov 2008